Multiscale Modeling of Malaria-Infected Red Blood Cells

Anil K. Dasanna, Ulrich S. Schwarz, Gerhard Gompper, and Dmitry A. Fedosov

Contents

A. K. Dasanna · U. S. Schwarz
BioQuant-Center for Quantitative Biology and Institute of Theoretical Physics, Heidelberg University, Heidelberg, Germany
e-mail: anil.dasanna@bioquant.uni-heidelberg.de; schwarz@thphys.uni-heidelberg.de

G. Gompper · D. A. Fedosov (✉)
Institute of Complex Systems and Institute for Advanced Simulation, Forschungszentrum Jülich, Jülich, Germany
e-mail: g.gompper@fz-juelich.de; d.fedosov@fz-juelich.de

W. Andreoni, S. Yip (eds.), *Handbook of Materials Modeling*,
https://doi.org/10.1007/978-3-319-50257-1_66-1

Abstract

Malaria is a parasitic disease which takes approximately half a million lives every year. The unicellular parasites are transmitted by mosquitoes and mainly affect vascular blood flow by invading red blood cells (RBCs). The pathogenicity of malaria primarily results from substantial changes in the stiffness of infected RBCs and their ability to adhere to endothelial cells and other circulating blood cells, leading to a substantial disruption of normal blood circulation and inflammation of the vascular endothelium. Multiscale modeling of malaria has proved to contribute significantly to the understanding of this devastating disease. In particular, modeling on the level of single infected RBCs allows quantification of their mechanics, cytoadherence, and individual as well as collective behavior in blood flow. Recent modeling advances in this direction are discussed. We show how computational models in malaria are validated and used for the interpretation of experimental observations or the establishment of new physical hypotheses. Such computational models have a strong potential to elucidate a number of physical mechanisms relevant for malaria and to aid in the development of novel diagnostic tools and treatment strategies.

1 Introduction

Malaria is a mosquito-borne disease caused by *Plasmodium* parasites (Miller et al. 2002). These are unicellular eukaryotic cells whose continuous battle with humans has left a larger imprint on our genome than any other infectious diseases. There exist several *Plasmodium* species, including *P. falciparum*, *P. vivax*, *P. ovale*, *P. malariae*, and *P. knowlesi*, which cause very different disease severity. *P. falciparum* (Pf) is considered to be the most dangerous form of the disease with several hundred thousand deaths per year worldwide. The life cycle of a parasite is schematically illustrated in Fig. 1. Motile sporozoites are injected into the human skin during a mosquito blood meal. After entering the bloodstream, the sporozoites travel to the liver and infect hepatocytes. Within about 2 weeks, tens of thousands of merozoites form and are then released into the bloodstream, where they invade red blood cells (RBCs). Following RBC invasion, merozoites multiply inside infected RBCs (iRBCs) for about 48 h and finally rupture the RBC membrane (Abkarian et al. 2011), releasing around 20 new merozoites into the bloodstream. At the same time, some merozoites develop into the sexual form called gametocytes, which can be taken up from the blood by mosquitoes. These gametocytes infect female mosquitoes, where they first develop in the gut and later move to the salivary glands. This completes the life cycle of malaria parasites.

Infection of RBCs by malaria parasites leads to significant stiffening of the iRBC membrane for the case of Pf parasites (Cranston et al. 1984; Diez-Silva et al. 2010). Membrane stiffening can be moderate for other malaria species. The intraerythrocytic development of Pf parasites includes three major stages, called ring (0–24 h), trophozoite (24–36 h), and schizont (40–48 h). During this development,

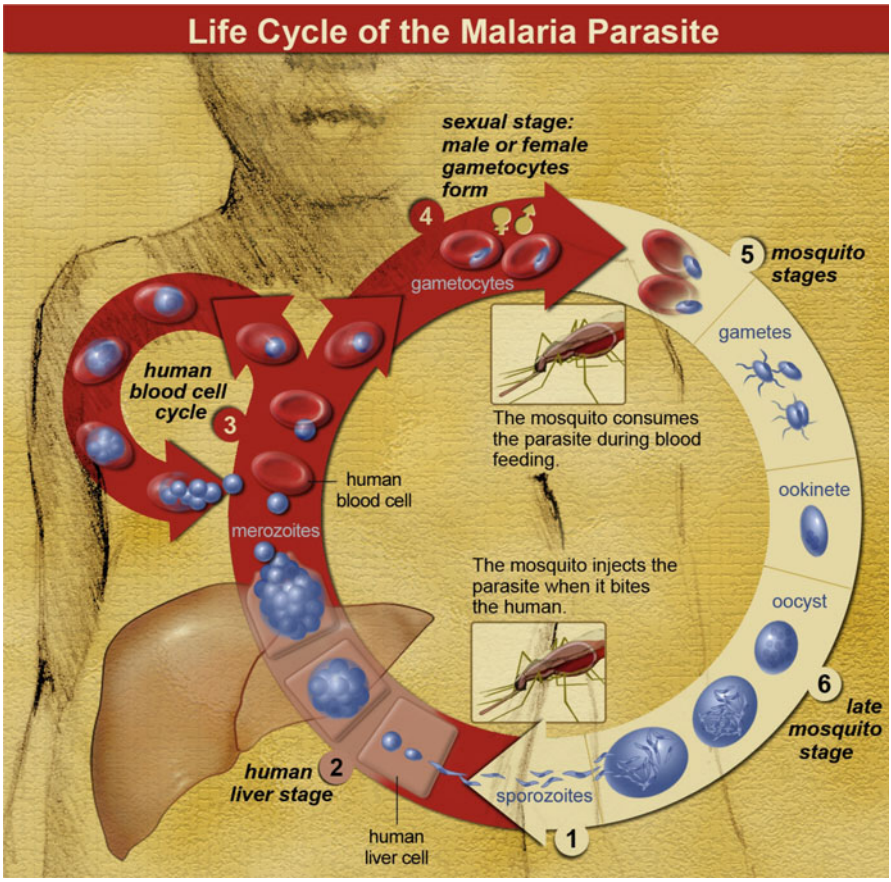

Fig. 1 The life cycle of malaria parasites. A mosquito infects a human host during a blood meal (stage 1). Then, malaria parasites in the form of sporozoites use blood vessels to reach the liver. They infect hepatocytes, develop into merozoites, and finally rupture the liver cells and enter the bloodstream again (stage 2). The merozoites invade RBCs, where they progress through the asexual intraerythrocytic stages, including ring, trophozoite, and schizont forms. Finally, RBCs are ruptured and new merozoites are released into the bloodstream, closing the asexual cycle in the blood (stage 3). Sexual forms are also produced in the blood (stage 4), which are taken up by a mosquito (stage 5), resulting in its infection and development in the gut (stage 6). They again become sporozoites and move to the salivary glands (stage 1), thus closing the malaria life cycle. From National Institute of Allergy and Infectious Diseases (NIAID)

the RBC membrane can stiffen by up to a factor of ten in comparison with healthy RBCs (Diez-Silva et al. 2010; Fedosov et al. 2011b). In addition, at the schizont stage iRBCs attain a near-spherical shape, since the parasites change the osmotic pressure inside the iRBC and also because they fill more and more of its volume. The stiffening and shape change of iRBCs impair their ability to deform and may lead to capillary occlusions (Cranston et al. 1984; Shelby et al. 2003).

Inside iRBCs, merozoites remain virtually invisible to the immune system. However, the membrane stiffening can be detected in the spleen, where RBCs have to squeeze through narrow slits as a part of the RBC quality control system (Engwerda et al. 2005; Pivkin et al. 2016). In order to survive at the late stages (trophozoite and schizont), parasites position adhesive proteins at the RBC membrane surface, which mediate cell adhesion to the endothelium (Brown et al. 1999; Miller et al. 2002). This mechanism delays or even prevents the passage of iRBCs through the spleen, allowing enough time for parasites to develop and rupture the cell membrane. Interestingly, the adhesive system induced by the parasite is similar to the way white blood cells (WBCs) adhere in the vasculature as a prerequisite for extravasating into the surrounding tissue, e.g., in the context of an infection (Helms et al. 2016). While WBCs use hundreds of microvilli with adhesive tips, iRBCs use thousands of adhesive knobs. In both cases, the protrusion from the surface seems essential to make contact with the endothelium (Korn and Schwarz 2006). Cytoadhesion is also the main reason for the absence of the late stages of iRBCs in patient blood samples, because adhesive cells remain immobile in the microvasculature. While cytoadhesion facilitates further progression of malaria, it has a strong potential for severe disruption of normal blood flow. Infected cells at the late stages are able to adhere not only to the vascular endothelium but also to other infected and healthy RBCs. Adherence of iRBCs is likely to be the main cause of bleeding complications in cerebral malaria due to blockages of small vessels in the brain (Adams et al. 2002). Cytoadherence also leads to inflammation of the vascular endothelium, which is an important part of the symptoms of the disease (Miller et al. 2002).

In this chapter, we focus on modeling various aspects of the malaria disease, using a multiscale computational framework. At the current stage, the multiscale approach to malaria already spans all relevant levels: from molecular aspects of RBC remodeling by the parasite to cell-level changes in mechanics and cytoadherence of iRBCs, and to the flow of many RBCs in complex geometries. Computational models are validated by comparison with a growing range of single-cell experiments under healthy and diseased conditions. Here, we discuss all levels of the multiscale problem of the blood stage of malaria. In particular, we discuss how the RBC is remodeled by the parasite. We then address modeling of RBC mechanics and the changes it experiences over the course of intraerythrocytic parasite development. Simulations of parasite invasion of RBCs and the cytoadherence of iRBCs at the late stages are described. Finally, we also review numerical efforts to understand blood rheology and flow in malaria and illustrate several microfluidic examples which can be utilized as novel devices for malaria detection and diagnosis. The computational modeling has proved to be a valuable tool in elucidating involved physical and biological mechanisms in malaria, and we discuss possible future steps, which can bring realistic simulations closer toward medical applications.

2 Methods and Models

2.1 Structure of Healthy and Infected Red Blood Cells

Healthy human RBCs have a biconcave shape with approximately 7.5–8.7 μm in diameter and 1.7–2.2 μm in thickness (Fung 1993). The RBC envelope consists of a phospholipid bilayer and a network of spectrin proteins (cytoskeleton) attached at the inner side of the bilayer via transmembrane proteins; see Fig. 2a. The spectrin network supplies shear elasticity to a RBC membrane, while the lipid bilayer serves as a barrier for exchange of solutes and provides resistance to bending and viscous damping when sheared. Human RBCs neither have organelles nor bulk cytoskeleton and are filled with a highly concentrated hemoglobin solution. Viscosity of the cytosol is about 6×10^{-3} Pa·s, while the plasma viscosity is approximately 1.2×10^{-3} Pa·s at a physiological temperature of 37 °C (Wells and Schmid-Schönbein 1969). Thus, the cytosol viscosity is about five times larger than that of the plasma under physiological conditions.

In comparison to healthy cells, iRBCs contain a growing parasitic body inside them. Furthermore, after the end of the ring stage or about halfway through the asexual cycle, the iRBC membrane starts developing adhesive protrusions on its surface, known as knobs, which are responsible for cytoadhesion. Knobs have been visualized using scanning electron microscopy (SEM) (Gruenberg et al. 1983) and atomic force microscopy (AFM) (Nagao et al. 2000; Quadt et al. 2012) during the different stages of the life cycle. These experiments have shown that the formation of knobs is strain-dependent and variable, with a density of about 10–30 knobs/μm^2 at the trophozoite stage and around 40–60 knobs/μm^2 at the schizont stage. The height of knobs remains nearly constant around 10–20 nm, while the knob diameter decreases from 160 to 100 nm (Gruenberg et al. 1983), when iRBCs progress from the trophozoite to the schizont stage.

2.2 Overview of Hydrodynamic Methods

Modeling blood flow in malaria requires mathematical formulations for fluid flow on the one side and blood cell shape and mechanics on the other side. Both blood plasma and RBC cytosol can be considered to be viscous Newtonian fluids. For microcirculatory blood flow, we deal with hydrodynamics at low Reynolds numbers, and therefore the Stokes equation has to be solved to describe fluid flow. For WBCs and iRBCs in the schizont stage, a spherical cell shape can be assumed and analytical solutions are available for the Stokes equation (Cichocki and Jones 1998). For the standard case of non-spherical RBCs, however, numerical approaches have to be employed. Fluid flow can be simulated by a variety of methods including continuum approaches based on the Navier-Stokes equations (Wendt 2009) and particle-based simulation methods, such as smoothed particle hydrodynamics (Monaghan 2005), dissipative particle dynamics (Pivkin et al. 2011), and multi-particle collision

dynamics (Gompper et al. 2009). Even though continuum techniques are often faster and more robust than particle-based methods, certain features such as thermal fluctuations and the inclusion of suspended complex structures (e.g., molecules and cells) are better suited for particle-based methods. Therefore, particle-based methods are very popular for the modeling of the dynamics of complex fluids such as blood.

2.3 Adhesive Dynamics of Spherical Cells

Modeling the motion of spherical cells, such as WBCs and iRBCs at the schizont stage (Helms et al. 2016; Dasanna et al. 2017), is mathematically much simpler than the motion of cells with a non-spherical shape. Adhesive dynamics of a spherical cell in shear flow can be described by the Langevin equation (Hammer and Apte 1992; Korn and Schwarz 2007) as

$$\partial_t X(t) = u^\infty + M\{\mathbf{F}_S + \mathbf{F}_D\} + k_B T \nabla M + \xi(t), \tag{1}$$

where $X(t)$ is a six-dimensional vector describing sphere translation and rotation, M is the mobility matrix, u^∞ is the imposed flow, and $\mathbf{F}_S$ and $\mathbf{F}_D$ denote shear (i.e., from fluid flow) and direct (e.g., gravity, adhesion) forces and torques, respectively. The term with ∇M is a non-zero spurious drift, since the mobility matrix depends on the sphere position. The last term $\xi(t)$ corresponds to a random force which represents thermal fluctuations and obeys the fluctuation-dissipation theorem with an equilibrium temperature T.

For cell adhesion, stochastic bond dynamics is modeled between receptors on the cell surface and ligands at the substrate. Bond association and dissociation are governed by on- and off-rates, k_{on} and k_{off}, respectively. Usually k_{on} is taken to be constant, and a bond with the rate k_{on} may form between a receptor and a ligand if the distance between them is less than a specified encounter distance r_0. For an existing bond, Bell's equation $k_{off} = k^0_{off} \exp(F/F_d)$ (Bell 1978) is used to model that most bonds dissociate faster under force F, with an internal force scale F_d. Mechanically, a bond is assumed to be a harmonic spring with a spring constant k_s and equilibrium bond length ℓ_0. The probability for bond association and dissociation is calculated as $P = 1 - \exp(-k\Delta t)$, where Δt is the time step employed in simulations.

2.4 Modeling Cell Deformation

In the general case of a non-spherical cell shape, hydrodynamic flow has to be combined with a deformable cell model. RBCs are modeled by a flexible network of springs with triangular elements (Seung and Nelson 1988; Noguchi and Gompper 2005; Fedosov et al. 2010), as shown in Fig. 2b. The free energy of the membrane is defined as

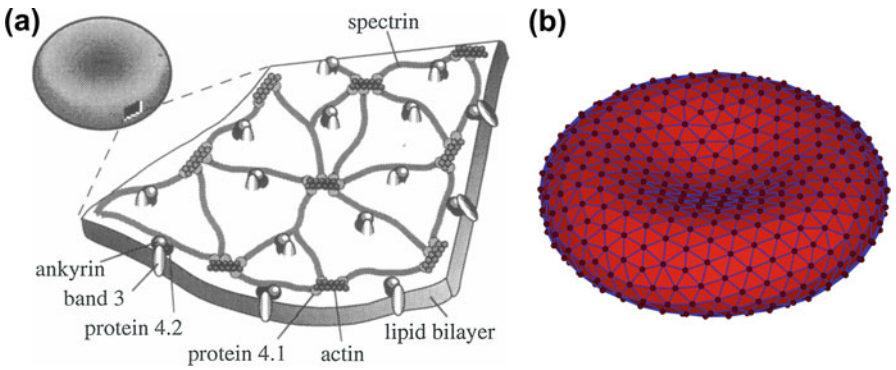

Fig. 2 (**a**) A schematic of the RBC membrane structure, showing the spectrin cytoskeleton being anchored to the lipid bilayer by transmembrane proteins (Reproduced with permission from Hansen et al. 1997). (**b**) Mesoscopic representation of a RBC membrane by a triangular network of mechanical bonds. For iRBCs, adhesive bonds are anchored at the vertices of this network (Reproduced with permission from Fedosov et al. 2014)

$$U_{\text{cell}} = U_s + U_b + U_{a+v}, \tag{2}$$

where U_s is the spring's potential energy to impose membrane shear elasticity, U_b is the bending energy to represent bending rigidity of a membrane, and U_{a+v} stands for the area and volume conservation constraints, which mimic area incompressibility of the lipid bilayer and incompressibility of the cytosol, respectively. Linear properties of a regular hexagonal network can be derived analytically, providing a relation between the model parameters and the membrane macroscopic properties (Seung and Nelson 1988; Fedosov et al. 2010). Similar to the adhesive dynamics for spherical cells, receptors can be placed at the spring network and on- and off-rates can be used to model adhesive interactions with the substrate (Fedosov et al. 2011a,b). More details on blood cell and flow modeling can be found in recent reviews (Li et al. 2013; Fedosov et al. 2014; Freund 2014).

3 Results

3.1 RBC Shapes and Mechanics

The biconcave shape of RBCs is controlled by the relative ratio between their membrane area and cell volume and by the membrane elastic properties. The volume of a RBC is about 35–40% smaller than the volume of a sphere with the same surface area. Thus, the reduced volume of a RBC is normally in the range between 0.6 and 0.65. Lipid vesicles with this reduced volume attain a biconcave shape which closely resembles that of RBCs (Seifert et al. 1991). In comparison to vesicles, RBC membrane also possesses shear elasticity supplied by the spectrin network.

This mechanical component is important to prevent budding of vesicles from the RBC membrane and membrane rupture under very large deformations. Therefore, the equilibrium shape of RBCs in general is determined by a minimum energy of both bending and shear-elastic contributions (Lim et al. 2002).

For both contributions to the Hamiltonian, it is not clear what the appropriate reference state should be. In case of the bending energy, it is important to consider whether a membrane has spontaneous curvature, especially because the RBC membrane is known to have very different compositions in the inner and outer leaflets. Most existing RBC models (Noguchi and Gompper 2005; Fedosov et al. 2010) assume the spontaneous curvature to be zero. A large enough spontaneous curvature can lead to a variety of different shapes (e.g., stomatocyte, echinocyte) and change the importance of bending and shear-elastic contributions (Lim et al. 2002). However, questions whether a human RBC membrane possesses a non-zero spontaneous curvature and whether this curvature would be isotropically distributed on the RBC surface still remain unanswered.

The reference state for the shear-elastic energy is generally referred to as stress-free shape of a RBC (Peng et al. 2014). It appears plausible to assume the biconcave shape of RBCs as the stress-free shape, because transmembrane proteins, which connect the spectrin network and the lipid bilayer, are able to diffuse within the bilayer, leading to a potential relaxation of existing elastic stresses. However, recent simulations (Peng et al. 2014) show that the assumption of biconcave stress-free shape leads to an incorrect prediction of the transition from tumbling dynamics to tank-treading dynamics of a RBC in shear flow. On the other hand, the assumption of a spherical stress-free shape results in a stomatocytic shape of the membrane for physiological values of RBC bending rigidity and shear elasticity (Li et al. 2005). An assumption of a spheroidal stress-free shape close to a sphere seems to be able to resolve these issues (Peng et al. 2014).

The mechanical properties of RBC membranes have been measured by a number of single-cell experimental techniques, including micropipette aspiration (Waugh and Evans 1979; Discher et al. 1994), deformation by optical tweezers (Henon et al. 1999; Suresh et al. 2005), optical magnetic twisting cytometry (Puig-de-Morales-Marinkovic et al. 2007), and three-dimensional measurement of membrane thermal fluctuations (Popescu et al. 2007; Park et al. 2008). Optical tweezers and micropipette aspiration methods apply a strong global deformation to the RBC membrane, while optical magnetic twisting cytometry and measurements of membrane thermal fluctuations correspond to local measurements. The two former techniques allow a measurement of the macroscopic shear modulus of a RBC membrane. Figure 3 presents a comparison between the deformation of a healthy RBC by optical tweezers (Suresh et al. 2005) and the corresponding numerical simulations (Fedosov et al. 2010). The numerical simulations mimic experimental conditions and allow the quantification of observed RBC deformation. A best fit (black line) between simulations and experiments is achieved for the two-dimensional (2D) Young's modulus of $Y = 18.9\,\mu$N/m and 2D shear modulus of $\mu = 4.73\,\mu$N/m. Note that this value of the shear modulus is in 2D such that $\mu \approx Y/4$, while Fedosov et al. (2010) provide a 3D value with $\mu \approx Y/3$.

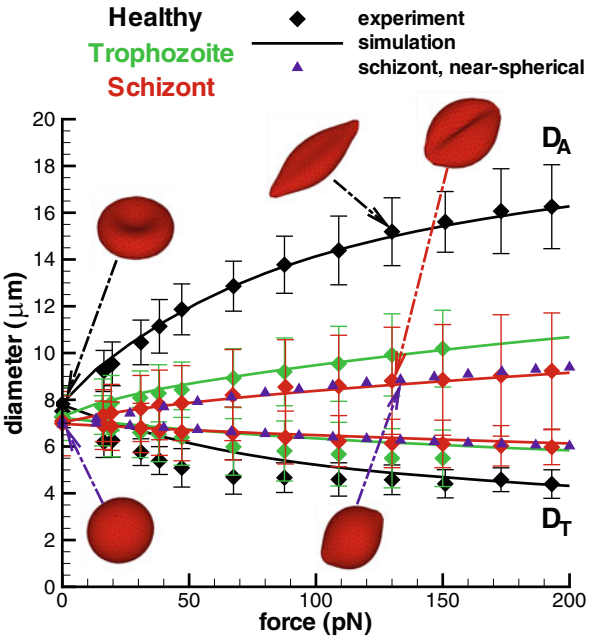

Fig. 3 Stretching response of a healthy RBC and iRBCs for different stages compared with the optical tweezers experiments (Suresh et al. 2005). D_A and D_T refer to the axial and transverse diameters (Reused with permission from Fedosov et al. 2011b)

Optical magnetic twisting cytometry (Puig-de-Morales-Marinkovic et al. 2007) allows the measurement of local rheological properties (e.g., the complex modulus) of a RBC membrane. Complex modulus consists of storage and loss moduli, which are determined by elastic and viscous properties of the membrane, respectively. Therefore, both bending rigidity and shear elasticity affect the storage modulus, while the loss modulus is associated with the viscosity of a membrane, cytosol, and suspending medium (Fedosov et al. 2010). Simulations performed to quantify the experimental data (Puig-de-Morales-Marinkovic et al. 2007) have yielded a value of $\kappa = 3 \times 10^{-19}$ J for the bending rigidity (about $70 k_B T$) and $\eta_m = 2.2 \times 10^{-8}$ Pa·s·m for the membrane viscosity (Fedosov et al. 2010). Measurements of membrane thermal fluctuations (Popescu et al. 2007; Park et al. 2008) are directly associated with the membrane characteristics; however, their reliable interpretation for RBCs still remains difficult. There exist large discrepancies between different studies, which are likely to originate from the approximations used in analytical models derived for planar and near-spherical membranes (Strey et al. 1995; Betz and Sykes 2012). Hence, a quantitative interpretation of fluctuation measurements requires reliable and accurate simulation models of a RBC.

A number of experiments with RBCs provide sufficient evidence for a complex membrane mechanical response including its unique viscoelastic properties.

In addition, it has been recognized that RBCs possess a metabolic activity through the consumption of adenosine triphosphate (ATP), which contributes to measured membrane flickering. The studies with ATP depletion (Betz et al. 2009; Park et al. 2010) have shown that membrane fluctuations decrease; however, during the ATP depletion process, there is no guarantee that RBCs are not subject to changes in membrane elasticity. In contrast, another investigation (Evans et al. 2008) has questioned the effect of ATP on measured flickering. A recent experimental and simulation study (Turlier et al. 2016) has provided compelling evidence for cell activity by testing directly the fluctuation-dissipation relation, which is valid for any system in equilibrium. A violation of the fluctuation-dissipation relation has been shown, and a contribution of active processes to the observed membrane flickering has been demonstrated (Turlier et al. 2016).

3.2 Mechanics of RBC Invasion by a Parasite

The first important step in the blood cycle of malaria is the invasion of RBCs by merozoites. Conceptually, this process can be divided into discrete steps, as shown schematically in Fig. 4a. Invasion commences with a low-affinity, long-range (12–40 nm), and nondirectional binding of a RBC by the merozoite, which then reorients such that its apex directly contacts the RBC. Then, formation of

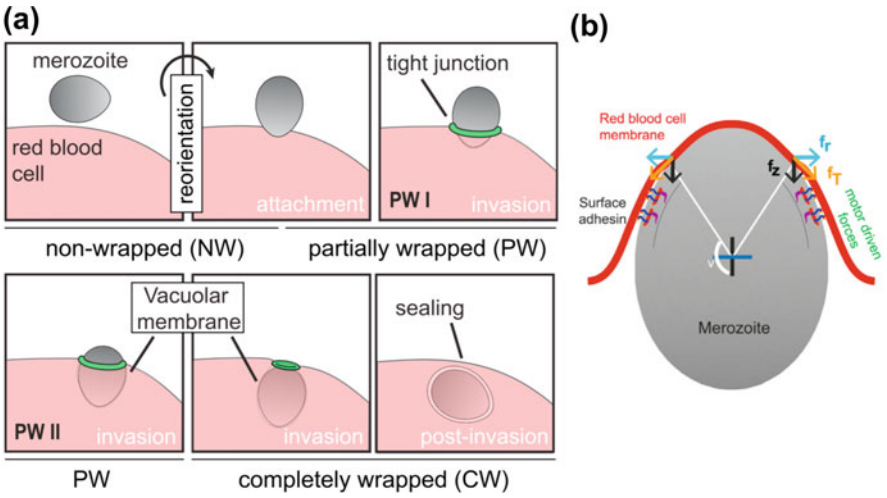

Fig. 4 (**a**) The stages of merozoite invasion. Schematic representation depicting different wrapping phases of the merozoite from reorientation and attachment through two partially wrapped states (with different wrapping fractions) to post-invasion. (**b**) Actomyosin force supports merozoite invasion. f_T is the force acting tangentially along the membrane surface as it wraps along the particle, whereas f_z is the component of this tangential force along the z axis whose role is to inject the particle into the membrane, while the component f_r is balanced by an equal force at the other side of the membrane (Reprinted with permission from Dasgupta et al. 2014b)

a close-range interaction (4 nm or less) leads to the establishment of a RBC-merozoite tight junction. This critical structure is the organizing nexus around which invasion events are orchestrated. It acts as the aperture through which the merozoite passes during invasion and segregates RBC membrane from an emerging vacuolar membrane (likely derived in part from the parasite membrane), which fuses to form the parasitophorous vacuole surrounding the parasite after invasion (Cowman et al. 2012).

The merozoite has a shape, very similar to a chicken egg, with a width-to-length ratio of 0.7, but with a characteristic length of only 2 μm (Dasgupta et al. 2014b). The adhesion and wrapping of spherical (Deserno 2004; Bahrami et al. 2016) and non-spherical (Dasgupta et al. 2013, 2014a) nano- and microparticles by membranes have been investigated quite intensively in recent years (Dasgupta et al. 2017). These theoretical and numerical approaches provide the basis for the modeling of merozoite invasion. Particles are expected to adhere to a membrane with its least-curved side, because this configuration provides the largest adhesion area with the lowest cost in membrane deformation energy. Therefore, the reorientation of the merozoite for apical invasion requires a nonuniform adhesion energy, with an adhesion maximum at the apex. This could be facilitated by a transient gradient of adhesive proteins from apex to base on the merozoite surface (Cowman et al. 2012). Once the tight junction has been formed, the wrapping of the merozoite is controlled by four energetic contributions: (i) the adhesion strength, (ii) the membrane bending rigidity and its spontaneous curvature, (iii) the lateral tension of the RBC membrane, and (vi) the effective line tension of the tight junction. Different invasion scenarios can be discussed on the basis of such a model (Dasgupta et al. 2014b). Obviously, if the adhesion strength is very large (or small) and the membrane tension is very low (or high), complete wrapping will always (or never) occur. Large adhesion strengths allow immediate complete wrapping and RBC entry, but might also be associated with unspecific binding to other membranes and problems associated with membrane surface-coat shedding. Thus, the most interesting scenario is where these various contributions nearly balance each other. Also, this scenario for merozoite invasion is plausible, because merozoites can successfully enter RBCs, but not with certainty. As an example, phase diagrams for parasite wrapping from Dasgupta et al. (2014b) show that for a fixed line tension, there is a non-wrapped state for small, reduced adhesive strength, two partial-wrapped states for intermediate adhesion, and a complete-wrapped state for large adhesive strength. The parasite can navigate in the phase diagram to move from the non-wrapped to the complete-wrapped state. For instance, it can move between the partial-wrapped states (shallow wrapped and deep wrapped) by reducing the membrane tension through secretion of unstructured lipids. There is indeed experimental evidence for such a process, the discharge of lipids from the rhoptry organelles (Hanssen et al. 2013; Bannister et al. 1986). Similarly, a change of the spontaneous curvature to a value more favorable for wrapping (e.g., by detachment of the spectrin cytoskeleton from the bilayer or its reorganization Kabaso et al. 2010) can induce a transition from the deep-wrapped to complete-wrapped state.

It is important to note that the transitions from shallow- to deep-wrapped states and from deep- to complete-wrapped states are associated with large energy barriers. Even though the complete-wrapped state is energetically favorable, it might be difficult to reach it from the deep-wrapped state. Thus, it is conjectured that the barrier crossing is facilitated by active processes. Indeed, there is a long-standing experimental evidence that activity of the parasite actomyosin motor governs successful host-cell entry (Angrisano et al. 2006). The current model for the source of parasite active motor force (see Fig. 4b) posits that an anchored myosin motor inside the parasite (tethered to the RBC cytoskeleton) transmits force directly through a short polymerized actin filament, which is linked to the surface-bound adhesins (Baum et al. 2006). The height of energy barrier obtained from the wrapping model described above now allows an estimate of the magnitude of the required motor activity, which indicates that a few 10s to a few 100s of motor proteins should suffice. Thus, even when membrane-wrapped states are stable, the essential role of the motor lies in overcoming energy barriers between the partial-wrapped and complete-wrapped states.

3.3 RBC Remodeling During Infection

The shapes of iRBCs can be measured, for example, by fluorescence confocal microscopy, and from these data surface area and volume can be deduced. An early study with restricted time resolution has reported relatively constant values (Esposito et al. 2010), in contrast to a colloid-osmotic model, which predicts the total volume of iRBCs to increase dramatically in the later stages (Lew et al. 2003; Mauritz et al. 2009). To resolve this issue, Waldecker et al. (2017) have reconstructed iRBC shapes over the whole intracellular cycle with a time interval of 4 h. Figure 5a shows typical shapes of iRBCs at different times, including the shape of the parasite inside. At the ring stage, the parasite is located at the rim of iRBC, causing a little bump along the edge of the cell. Starting from the trophozoite stage, parasite begins to multiply and the overall parasitic volume increases. At the end of the life cycle, iRBC reaches a nearly spherical shape with around 20 parasites inside the cell. The corresponding changes in the iRBC and parasite volume are quantified in Fig. 5b. The experimental measurements agree well with the predictions of the colloid-osmotic model, which are shown by solid lines (Mauritz et al. 2009; Lew et al. 2003). While the volume increases by 60%, the surface area remains nearly constant throughout the life cycle.

Starting around the midpoint of development, iRBCs induce adhesive protrusions at the membrane, which significantly modify the structure of the iRBC cytoskeleton. Shi et al. (2013) performed AFM imaging of inverted iRBCs to study the changes in the spectrin network during infection, as shown in Fig. 6a. The average length of spectrin filaments is found to be 43 ± 5 nm for healthy RBCs, whereas for the ring stage, the spectrin-filament length becomes about 48 ± 7 nm. For the middle trophozoite stage, the length is 64 ± 9 nm, and for the schizont stage, it is about 75 ± 11 nm, which is roughly twice the spectrin length of healthy RBCs.

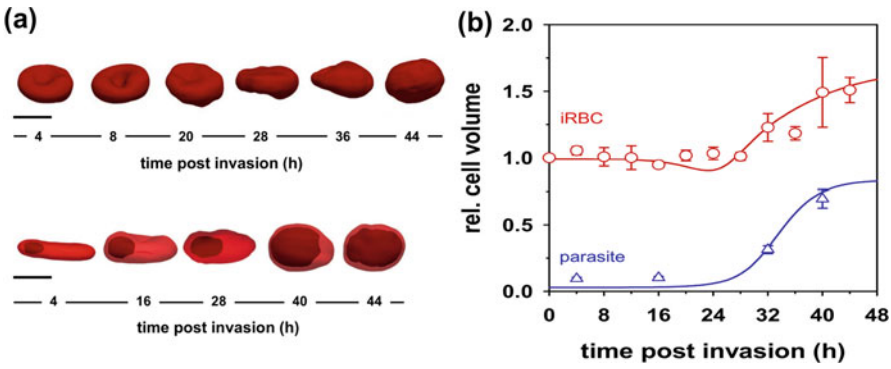

Fig. 5 (**a**) Reconstructed shapes from confocal images of iRBCs at different times of the parasite development. The bottom row shows the shapes of a growing parasite inside the iRBC at various times. Scale bar is 5 μm. (**b**) Relative cell volume and parasite volume as a function of post-infection time. The solid lines are predictions by the osmotic colloid model (Reused with permission from Waldecker et al. 2017)

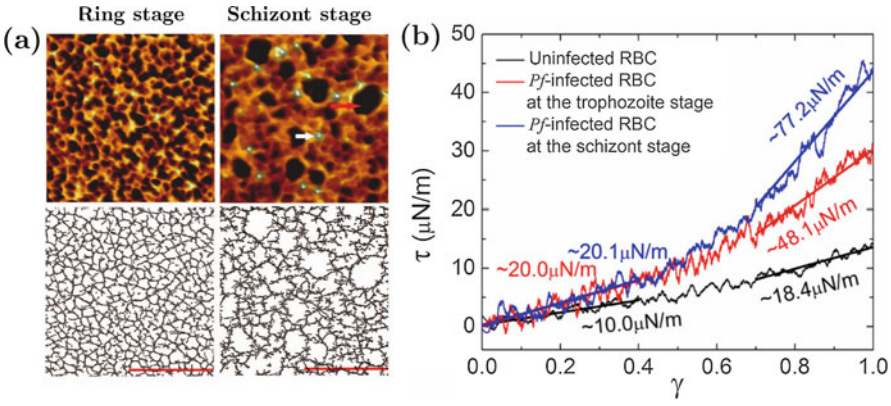

Fig. 6 (**a**) AFM images of spectrin cytoskeleton and image-processed representations for ring and schizont stages. Scale bar is 500 nm. The red arrow in schizont AFM image indicates a hole region, while the white arrow points to a knob Reused with permission from Shi et al. 2013). (**b**) Shear stress-strain response curves for uninfected and infected RBCs from mesoscopic model of RBC membrane (Reused with permission from Zhang et al. 2015)

In addition, spectrin filaments are found to accumulate at the knob areas, but they become sparser in non-knobby areas. Zhang et al. (2015) have studied the effect of knobs and enhanced coupling between plasma membrane and spectrin network using coarse-grained simulations based on these observations. Knobs were modeled as stiff regions of plasma membrane, and coupling between the plasma membrane and spectrin network was increased at the knobby areas. Simulation of the strain response of this composite membrane to shear stress results in the estimation of shear modulus for uninfected and infected RBCs. Figure 6b shows

shear stress-strain response curves for uninfected, trophozoite, and schizont stages with the 2D shear moduli (at large shear strains) $\mu \simeq 18\,\mu$N/m, $\mu \simeq 48\,\mu$N/m, and $\mu \simeq 78\,\mu$N/m, respectively, which are close to values reported in experiments (Suresh et al. 2005). In general, the simulations show strong strain-hardening effects, presumably due to the polymer nature of the spectrin.

3.4 RBC Mechanics During Infection

Progressive stiffening of iRBCs has been measured by optical tweezers (Suresh et al. 2005) and by diffraction phase microscopy through monitoring thermal fluctuations (Park et al. 2008). Figure 3 shows a comparison of RBC stretching between simulation results for healthy and infected RBCs at different stages and experimental results (Suresh et al. 2005). Fitting of RBC stretching in simulations to the experimental data leads to 2D shear moduli $\mu = 14.5\,\mu$N/m for the ring stage, $\mu = 29\,\mu$N/m for the trophozoite, and $\mu = 40\,\mu$N/m for the schizont (Fedosov et al. 2011b). Note that the geometry of an iRBC at the schizont stage is taken to be of ellipsoidal shape with the axes $a_x = a_y = 1.2a_z$, which is not very far from a sphere. Taking a biconcave shape for the schizont stage in simulations results into a prediction with a larger shear modulus than that for the near-spherical shape. In the case of the deflated biconcave shape, the form of an iRBC is altered first in response to stretching and followed by membrane deformation, while for the near-spherical shape, the fluid restricts shape deformation and membrane stretching has to occur right away. In conclusion, the cell geometry plays an important role in the quantification of experimental data.

3.5 Adhesion of Infected Cells

Adhesion of iRBCs lies at the heart of parasite survival, as it prevents elimination of iRBCs in the spleen. Adhesive receptors on iRBC surface (PfEMP-1 encoded by the family of var genes) are localized to the knobs and can bind multiple ligands (mainly ICAM-1 and CD36) on vascular endothelial cells. The precise roles of different ligands in iRBC adhesion are quite complex, as the knob receptors bind to the various ligands with distinct adhesion strength (Yipp et al. 2000). For instance, experiments with flow assays hint at an increase of ICAM-1 adherence of iRBCs with shear stress (i.e., displaying characteristics of a catch bond), while CD36 does not show this behavior (Nash et al. 1992). Enhancement of adhesion under flow is not uncommon for cells in shear flow, including WBCs and bacteria, and has been demonstrated for iRBCs adhering to supported bilayers (Rieger et al. 2015). Experiments using single-bond force spectroscopy (Lim et al. 2017) have shown that iRBCs form slip bonds with CD36 and catch bonds with ICAM-1, as suggested before by flow chamber experiments. The characteristic rupture force for both slip and catch bonds is close to 10 pN, which is also comparable with the force for WBC bonds in the range of 10–50 pN (Marshall et al. 2003; Hanley et al. 2004). On the

modeling side, the slip bond can be simulated by Bell's model (Bell 1978), while the catch bond is often described by Dembo's model (Dembo et al. 1988).

The standard model for the adhesion of single cells under flow has been established with adhesive dynamics for round cells. Originally developed for WBCs (Hammer and Apte 1992; Korn and Schwarz 2007), this approach has recently been applied to iRBCs at the schizont stage (Helms et al. 2016; Dasanna et al. 2017). A phase diagram with different dynamic states (free motion, transient adhesion, rolling adhesion, and firm adhesion) has been simulated for the slip-bond model as a function of molecular on- and off-rates (Korn and Schwarz 2008; Helms et al. 2016), which can serve as a reference case to interpret experimental data. In the rolling adhesion regime, rolling velocity as a function of shear rate can be used to estimate molecular data. Hence, it has been estimated that ICAM-1 receptor distance should be between 100 and 400 nm to yield the observed rolling velocity around 100 μm/s at a shear rate of about $100\,s^{-1}$ (Dasanna et al. 2017).

An interesting aspect of iRBC adhesive motion is the nature of single trajectories, which often displays an oscillatory pattern in velocity and has been studied both numerically and in experiments (Fedosov et al. 2011a; Dasanna et al. 2017). Unlike WBCs, iRBCs have a non-spherical shape for the majority of parasite's life cycle, except the schizont stage. Mesoscopic modeling of iRBCs (Fedosov et al. 2011a) has demonstrated that cells at the trophozoite stage flip rather than roll on a substrate because of their discoid shape. For a Young's modulus similar to that of healthy RBCs, crawling motion is observed, while a large enough Young's modulus (more than three times that of healthy RBCs) leads to a rather regular flipping motion. The flipping may become less regular with the presence of parasite inside the cytosol (Fedosov et al. 2011a). Figure 7a shows snapshots of RBC motion for the three cases: (top) a crawling cell with a Young's modulus of $Y = 18.9\,\mu$N/m, (middle) a flipping iRBC with a Young's modulus of $Y = 168\,\mu$N/m, and (bottom) a flipping cell with a parasite body inside. Dasanna et al. (2017) have studied rolling adhesion of iRBCs at the trophozoite and schizont stages on endothelial cells in flow chamber experiments. The effect of the parasite on the iRBC rolling dynamics has been investigated, and therefore both the iRBC and fluorescently labeled parasite were tracked. Figure 7b presents translational velocity and fluorescence amplitude of the parasite inside the iRBC for a rolling trophozoite. The elliptic markings of the peaks in velocity and fluorescence amplitude indicate the anticorrelation between them, which is significant for flipping. Thus, when the iRBC starts a flip, the parasite moves away from the substrate (fluorescence amplitude thereby decreases), and when it comes down, the fluorescent amplitude increases. It has been also shown that this anticorrelation disappears and the fluorescent amplitude does not oscillate for iRBCs at the schizont stage, as they are round and rigid, so that the flipping transforms to rolling. Rolling velocities of schizont-stage iRBCs are found to be smaller than those of trophozoites, presumably because of the larger number of knobs (Dasanna et al. 2017).

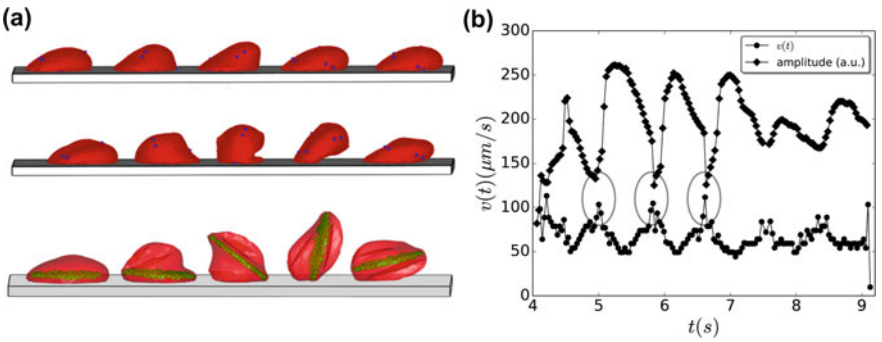

Fig. 7 (**a**) Snapshots of modeled flipping iRBCs with a small membrane Young's modulus (top), a large Young's modulus (middle), and, when it contains a rigid body, imitating the presence of parasite (bottom) (Reused with permission from Fedosov et al. 2011a). (**b**) Representative trajectory of a rolling trophozoite cell on endothelial layer, showing cell velocity and fluorescence intensity of the parasite inside the iRBC (Reused with permission from Dasanna et al. 2017)

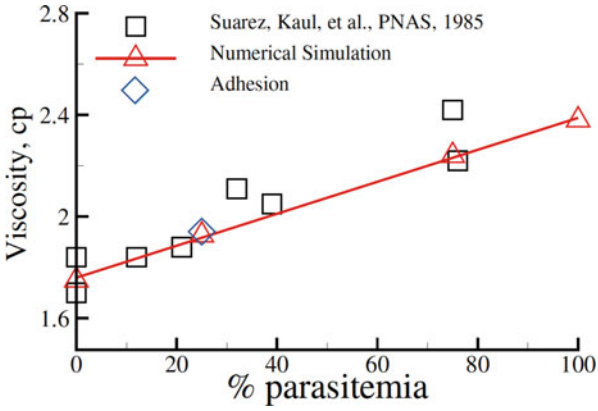

Fig. 8 Viscosity of the malaria-infected blood at hematocrit 30% for different parasitemias in comparison to experimental data (Raventos-Suarez et al. 1985). The diamond symbol corresponds to a simulation with aggregation interactions among RBCs (Reused with permission from Fedosov et al. 2011c)

3.6 Blood Rheology in Malaria

Bulk viscosity of blood is a macroscopic characteristic that depends on single-cell properties and their collective interactions (Fedosov et al. 2011d; Lanotte et al. 2016). The bulk viscosity of blood in malaria increases with the parasitemia level (or fraction of iRBCs) because of the increased stiffness of iRBCs (Raventos-Suarez et al. 1985) in comparison to healthy RBCs. A significant viscosity increase leads to an increased blood flow resistance and a reduced blood perfusion. Numerical simulations (Fedosov et al. 2011b) predict an increase of blood flow resistance in microvessels in malaria up to 50% for high parasitemia levels.

Bulk viscosity of infected blood in malaria for different parasitemia levels, hematocrit 30%, and shear rate $230\,s^{-1}$ has been measured experimentally (Raventos-Suarez et al. 1985) and estimated in simulations (Fedosov et al. 2011c), as shown in Fig. 8. In the simulations, infected blood is modeled as a suspension of healthy and

infected RBCs at the schizont stage with $\mu = 40\,\mu$N/m. The simulated viscosity as a function of the parasitemia is in excellent agreement with the corresponding experimental data, which show a roughly linear dependence of the infected blood viscosity on parasitemia level.

iRBCs adhere not only to the endothelium but also to other healthy and infected RBCs. Simulations with attractive interactions between infected and healthy RBCs for the parasitemia of 25% show that the blood viscosity does not increase significantly (see Fig. 8). This is likely due to the fact that the simulated shear rate is high enough to disperse RBCs within the suspension and to diminish aggregation effects on the bulk viscosity. Thus, a much stronger effect of the aggregation interactions should be expected at low shear rates. Furthermore, iRBCs at later stages form specific bonds with other cells, which should generally be stronger than the attractive interactions modeled by Fedosov et al. (2011c).

3.7 Blood Flow in Malaria

It is intuitive that blood flow resistance in malaria should increase due to an elevated stiffness of iRBCs and their cytoadherence. A simple model for the estimation of blood flow resistance is Poiseuille flow of blood in tubes, which mimics blood flow in microvessels. Blood flow in malaria has been simulated as a suspension of healthy and infected RBCs at the trophozoite stage ($\mu = 29\,\mu$N/m) and hematocrit 45%. Figure 9 shows the relative apparent viscosity in malaria for several parasitemia levels from 25% to 100% and microvessels with diameters 10 µm and 20 µm. The relative apparent viscosity is computed as $\eta_{\text{rel}} = \eta_{\text{app}}/\eta_s$, where η_s is the plasma viscosity and $\eta_{\text{app}} = \pi \Delta P D^4/(128 Q L)$ is the apparent viscosity. Here, ΔP is the pressure difference, Q is the flow rate, and L is the length of the tube. The relative apparent viscosity is a measure of flow resistance, as it compares apparent viscosity of blood with the viscosity of blood plasma.

The inset of Fig. 9 shows a snapshot of RBCs flowing in a tube of diameter 20 µm at a parasitemia level of 25%. The effect of parasitemia level on the flow resistance in Fig. 9 appears to be more prominent for small diameters and high hematocrit values. Thus, at $H_t = 45\%$ blood flow resistance in malaria may increase up to 50% in vessels of diameters around 10 µm and up to about 40% for vessel diameters around 20 µm. Note that these increases do not include any contributions from the adhesive interactions between iRBCs and other cells. Therefore, the inclusion of cytoadhesion would result in a further increase in blood flow resistance in malaria.

3.8 Malaria and Microfluidics

Microfluidic devices offer unique opportunities for the detection and manipulation of different suspended particles and cells. One of the first observations of iRBCs in microfluidics is a study of the passage of iRBCs through small constrictions driven by fluid flow (Shelby et al. 2003). The experiments have been performed for

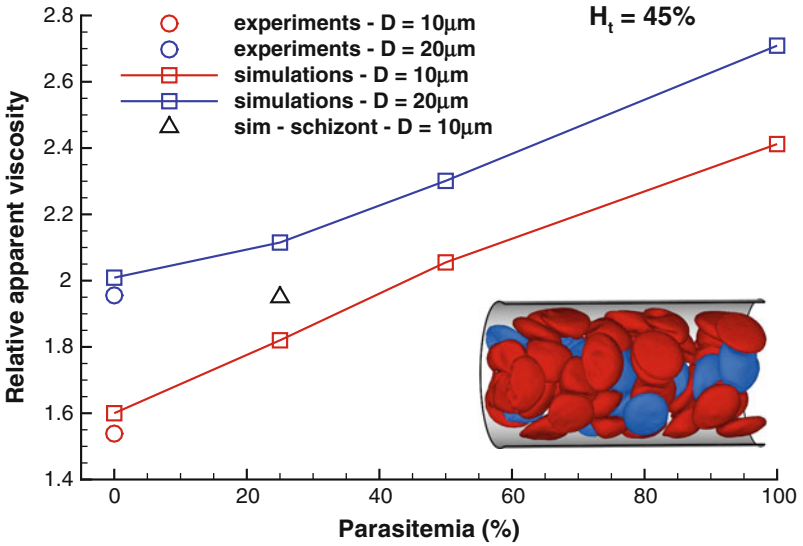

Fig. 9 Flow resistance in malaria. Healthy (red) and infected RBCs (blue) in tube flow with a diameter $D = 20\,\mu$m, hematocrit 45%, and parasitemia 25%. The relative apparent viscosity of blood in malaria is plotted for various parasitemia levels and tube diameters. Triangle symbol corresponds to the schizont stage with a near-spherical shape. Experimental data from the empirical fit are from Pries et al. (1992)

different channel sizes and stages of parasite development and have shown that the late stages, such as trophozoite and schizont, may result in blockage of microvessels with diameters smaller than about 6 μm. Corresponding simulation studies (Imai et al. 2010; Wu and Feng 2013) have also come to a similar conclusion, suggesting that the smallest vessel in the microvasculature can be blocked by single iRBCs in the trophozoite and schizont stages.

The filtration concept has been also employed in another microfluidic device with many obstacles (Bow et al. 2011), where both healthy and infected RBCs are able to pass constriction geometries (no blockage is observed). However, iRBCs exhibit lower average velocities in comparison to healthy RBCs. This speed difference between healthy and infected RBCs is attributed to an increased membrane stiffness and viscosity of the iRBCs in comparison to healthy cells. Deformability-based sorting has been also proposed in the context of deterministic lateral displacement (DLD) microfluidic devices (Henry et al. 2016; Krüger et al. 2014). DLDs utilize micropost arrays, which have been originally designed to continuously sort spherical colloidal particles according to their size (Davis et al. 2006; Holm et al. 2011). However, DLDs do not directly follow the filtration concept, because the gaps between the posts are generally larger than suspended cells, as shown in Fig. 10. Sorting in DLDs is achieved by invoking differences in cell deformation and dynamics, which determine the trajectories of the cells within DLD devices (Henry et al. 2016; Krüger et al. 2014). For example, in Fig. 10, the differences in RBC

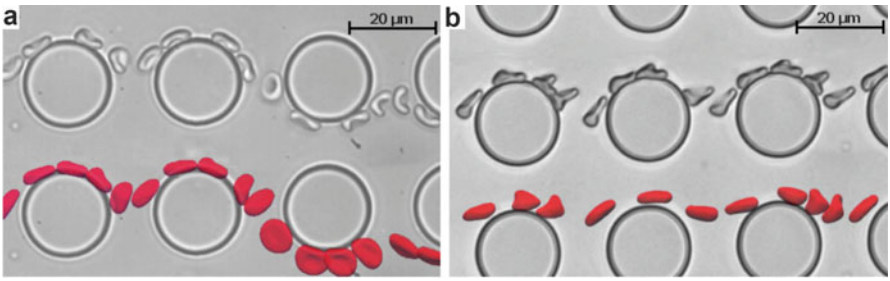

Fig. 10 Stroboscopic images of RBC deformation in a DLD device, taken from simulations and experiments. The viscosity contrast C between the cell's cytosol and suspending medium, which is (**a**) $C = 5$ and (**b**) $C = 1$, affects RBC dynamics and determines its traversal through the device (Reused with permission from Henry et al. 2016)

trajectories within the DLD device are governed by different viscosity contrasts between the RBC cytosol and suspending medium. Hence, a proper tuning of DLD device geometry and flow conditions can turn them into accurate and precise deformability-based sensors useful in the context of malaria.

4 Discussion and Outlook

The development of quantitative models for malaria infections is very important, because they allow the explanation of experimental results, the testing of various hypotheses, and the proposition of new biophysical mechanisms in disease development and progression. Due to the long evolutionary history of malaria and its complicated life cycle, this is not an easy task and it requires close cooperation between theoreticians and experimentalists. In particular, future studies have to further incorporate molecular information, for example, the molecular details of how the spectrin network is remodeled by the parasite, and the exact nature of the adhesion receptors localized to the knobs and their ligand counterparts in the vascular endothelium.

From the conceptual point of view, the most important aspect of malaria modeling is the multiscale nature of blood flow, which involves a wide range of spatiotemporal scales starting from single molecules for parasite-RBC interactions and the adhesion of iRBCs, to the deformation and dynamics of single cells, and, finally, to multicellular flow in large microvascular networks. Current models have proven to be sophisticated enough to be used successfully for the quantification of experiments with a few blood cells. Computational models of blood flow rapidly move to multicellular problems and already attempt to go beyond experimental predictions by generating and testing new physical and biological hypotheses. Thus, such simulations can be used to guide and optimize experimental settings for biophysical investigations and disease diagnosis (e.g., microfluidic devices).

Modeling of the malaria disease is very challenging, and many open questions remain, even in the context of the advances achieved over recent years, ranging from molecular mechanisms to cell deformation and adhesion under realistic blood flow conditions in the microcirculation. For instance, it is not fully understood how parasite can efficiently reorient itself after the initial random adhesion and then invade RBCs. Furthermore, exact changes and modifications of RBC membrane stiffness and cytoadherence by the parasite during its development need to be determined. In addition, it is unclear how the developing parasite, which can be thought of as a rigid-like body inside a RBC, affects the cell behavior in flow. Another important direction for future research concerns the characterization of the adhesive interactions between iRBCs and healthy RBCs, other blood cells (e.g., WBCs), and the endothelium, as this input is needed for realistic malaria modeling. Answers to these open questions for a single cell will allow the progression toward realistic modeling of blood flow in malaria, where a mixture of healthy and infected RBCs at different stages and complex flow geometries have to be generally considered.

Even though the impact of numerical modeling on malaria diagnosis and treatment is still rather limited, the development of new quantitative models and their application in practice acquire more and more momentum. Computational models have a great potential to provide guidance on how to improve disease detection and treatment and to optimize existing therapeutic tools, for instance, by introducing novel microfluidic approaches. Another substantial advancement needed for computational models is the development of predictive simulation approaches, which enable the modeling of long-time disease progression. This development requires the improvement of current models to much longer time scales including the ability of modeling various dynamic processes (e.g., parasite invasion, intra-RBC parasite development, dynamic adhesion changes).

Acknowledgements A.K.D. and U.S.S. acknowledge support by the DFG Collaborative Research Center 1129 on “Integrative Analysis of Pathogen Replication and Spread.” G.G. and D.A.F acknowledge the FP7-PEOPLE-2013-ITN LAPASO “Label-free particle sorting” for financial support. D.A.F acknowledges funding by the Alexander von Humboldt Foundation. G.G. and D.A.F also gratefully acknowledge a CPU time grant by the Jülich Supercomputing Center.

References

Abkarian M, Massiera G, Berry L, Roques M, Braun-Breton C (2011) A novel mechanism for egress of malarial parasites from red blood cells. Blood 117:4118–4124

Adams S, Brown H, Turner G (2002) Breaking down the blood-brain barrier: signaling a path to cerebral malaria? Trends Parasitol 18:360–366

Angrisano F, Riglar DT, Sturm A, Volz JC, Delves MJ, Zuccala ES, Turnbull L, Dekiwadia C, Olshina MA, Marapana DS, Wong W, Mollard V, Bradin CH, Tonkin CJ, Gunning PW, Ralph SA, Whitchurch CB, Sinden RE, Cowman AF, McFadden GI, Baum J (2006) Spatial localization of actin filaments across developmental stages of the malaria parasite. PLoS ONE 7:e32188

Bahrami AH, Lipowsky R, Weikl TR (2016) The role of membrane curvature for the wrapping of nanoparticles. Soft Matter 12:581–587

Bannister LH, Mitchell GH, Butcher GA, Dennis ED (1986) Lamellar membranes associated with rhoptries in erythrocytic merozoites of Plasmodium knowlesi: a clue to the mechanism of invasion. Parasitology 92:291–303

Baum J, Papenfuss AT, Baum B, Speed TP, Cowman AF (2006) Regulation of apicomplexan actin-based motility. Nat Rev Microbiol 4:621–628

Bell GI (1978) Models for the specific adhesion of cells to cells. Science 200:618–627

Betz T, Sykes C (2012) Time resolved membrane fluctuation spectroscopy. Soft Matter 8:5317–5326

Betz T, Lenz M, Joanny JF, Sykes C (2009) ATP-dependent mechanics of red blood cells. Proc Natl Acad Sci USA 106:15320–15325

Bow H, Pivkin IV, Diez-Silva M, Goldfless SJ, Dao M, Niles JC, Suresh S, Han J (2011) A microfabricated deformability-based flow cytometer with application to malaria. Lab Chip 11:1065–1073

Brown H, Hien TT, Day N, Mai NTH, Chuong LV, Chau TTH, Loc PP, Phu NH, Bethell D, Farrar J, Gatter K, White N, Turner G (1999) Evidence of blood-brain barrier dysfunction in human cerebral malaria. Neuropathol Appl Neurobiol 25:331–340

Cichocki B, Jones RB (1998) Image representation of a spherical particle near a hard wall. Phys A 258:273–302

Cowman AF, Berry D, Baum J (2012) The cellular and molecular basis for malaria parasite invasion of the human red blood cell. J Cell Biol 198:961–971

Cranston HA, Boylan CW, Carroll GL, Sutera SP, Williamson JR, Gluzman IY, Krogstad DJ (1984) Plasmodium falciparum maturation abolishes physiologic red cell deformability. Science 223:400–403

Dasanna AK, Lansche C, Lanzer M, Schwarz US (2017) Rolling adhesion of schizont stage malaria-infected red blood cells in shear flow. Biophys J 112:1908–1919

Dasgupta S, Auth T, Gompper G (2013) Wrapping of ellipsoidal nano-particles by fluid membranes. Soft Matter 9:5473–5482

Dasgupta S, Auth T, Gompper G (2014a) Shape and orientation matter for the cellular uptake of nonspherical particles. Nano Lett 14:687–693

Dasgupta S, Auth T, Gov N, Satchwell TJ, Hanssen E, Zuccala ES, Riglar DT, Toye AM, Betz T, Baum J, Gompper G (2014b) Membrane-wrapping contributions to malaria parasite invasion of the human erythrocyte. Biophys J 107:43–54

Dasgupta S, Auth T, Gompper G (2017) Nano- and microparticles at biological and fluid interfaces. J Phys Condens Matter 29:373003

Davis JA, Inglis DW, Morton KJ, Lawrence DA, Huang LR, Chou SY, Sturm JC, Austin RH (2006) Deterministic hydrodynamics: taking blood apart. Proc Nat Acad Sci USA 103:14779–14784

Dembo M, Torney DC, Saxman K, Hammer D (1988) The reaction-limited kinetics of membrane-to-surface adhesion and detachment. Proc R Soc Lond B 234:55–83

Deserno M (2004) Elastic deformation of a fluid membrane upon colloid binding. Phys Rev E 69:031903

Diez-Silva M, Dao M, Han J, Lim CT, Suresh S (2010) Shape and biomechanical characteristics of human red blood cells in health and disease. MRS Bull 35:382–388

Discher DE, Mohandas N, Evans EA (1994) Molecular maps of red cell deformation: hidden elasticity and in situ connectivity. Science 266:1032–1035

Engwerda CR, Beattie L, Amante FH (2005) The importance of the spleen in malaria. Trends Parasitol 21:75–80

Esposito A, Choimet JB, Skepper JN, Mauritz JMA, Lew VL, Kaminski CF, Tiffert T (2010) Quantitative imaging of human red blood cells infected with Plasmodium falciparum. Biophys J 99:953–960

Evans J, Gratzer W, Mohandas N, Parker K, Sleep J (2008) Fluctuations of the red blood cell membrane: relation to mechanical properties and lack of ATP dependence. Biophys J 94:4134–4144

Fedosov DA, Caswell B, Karniadakis GE (2010) A multiscale red blood cell model with accurate mechanics, rheology, and dynamics. Biophys J 98:2215–2225
Fedosov DA, Caswell B, Karniadakis GE (2011a) Wall shear stress-based model for adhesive dynamics of red blood cells in malaria. Biophys J 100:2084–2093
Fedosov DA, Caswell B, Suresh S, Karniadakis GE (2011b) Quantifying the biophysical characteristics of Plasmodium-falciparum-parasitized red blood cells in microcirculation. Proc Natl Acad Sci USA 108:35–39
Fedosov DA, Lei H, Caswell B, Suresh S, Karniadakis GE (2011c) Multiscale modeling of red blood cell mechanics and blood flow in malaria. PLoS Comput Biol 7:e1002270
Fedosov DA, Pan W, Caswell B, Gompper G, Karniadakis GE (2011d) Predicting human blood viscosity in silico. Proc Natl Acad Sci USA 108:11772–11777
Fedosov DA, Noguchi H, Gompper G (2014) Multiscale modeling of blood flow: from single cells to blood rheology. Biomech Model Mechanobiol 13:239–258
Freund JB (2014) Numerical simulation of flowing blood cells. Annu Rev Fluid Mech 46:67–95
Fung YC (1993) Biomechanics: mechanical properties of living tissues, 2nd edn. Springer, New York
Gompper G, Ihle T, Kroll DM, Winkler RG (2009) Multi-particle collision dynamics: a particle-based mesoscale simulation approach to the hydrodynamics of complex fluids. Adv Polym Sci 221:1–87
Gruenberg J, Allred DR, Sherman IW (1983) Scanning electron microscope-analysis of the protrusions (knobs) present on the surface of Plasmodium falciparum-infected erythrocytes. J Cell Biol 97:795–802
Hammer DA, Apte SM (1992) Simulation of cell rolling and adhesion on surfaces in shear flow: general results and analysis of selectin-mediated neutrophil adhesion. Biophys J 63:35–57
Hanley WD, Wirtz D, Konstantopoulos K (2004) Distinct kinetic and mechanical properties govern selectin-leukocyte interactions. J Cell Sci 117:2503–2511
Hansen JC, Skalak R, Chien S, Hoger A (1997) Influence of network topology on the elasticity of the red blood cell membrane skeleton. Biophys J 72:2369–2381
Hanssen E, Dekiwadia C, Riglar DT, Rug M, Lemgruber L, Cowman AF, Cyrklaff M, Kudryashev M, Frischknecht F, Baum J, Ralph SA (2013) Electron tomography of Plasmodium falciparum merozoites reveals core cellular events that underpin erythrocyte invasion. Cell Microbiol 15:1457–1472
Helms G, Dasanna AK, Schwarz US, Lanzer M (2016) Modeling cytoadhesion of Plasmodium falciparum-infected erythrocytes and leukocytes-common principles and distinctive features. FEBS Lett 590:1955–1971
Henon S, Lenormand G, Richert A, Gallet F (1999) A new determination of the shear modulus of the human erythrocyte membrane using optical tweezers. Biophys J 76:1145–1151
Henry E, Holm SH, Zhang Z, Beech JP, Tegenfeldt JO, Fedosov DA, Gompper G (2016) Sorting cells by their dynamical properties. Sci Rep 6:34375
Holm SH, Beech JP, Barrett MP, Tegenfeldt JO (2011) Separation of parasites from human blood using deterministic lateral displacement. Lab Chip 11:1326–1332
Imai Y, Kondo H, Ishikawa T, Lim CT, Yamaguchi T (2010) Modeling of hemodynamics arising from malaria infection. J Biomech 43:1386–1393
Kabaso D, Shlomovitz R, Auth T, Lew VL, Gov NS (2010) Curling and local shape changes of red blood cell membranes driven by cytoskeletal reorganization. Biophys J 99:808–816
Korn C, Schwarz US (2006) Efficiency of initiating cell adhesion in hydrodynamic flow. Phys Rev Lett 97:138103
Korn CB, Schwarz US (2007) Mean first passage times for bond formation for a Brownian particle in linear shear flow above a wall. J Chem Phys 126:095103
Korn CB, Schwarz US (2008) Dynamic states of cells adhering in shear flow: from slipping to rolling. Phys Rev E 77:041904
Krüger T, Holmes D, Coveney PV (2014) Deformability-based red blood cell separation in deterministic lateral displacement devices – a simulation study. Biomicrofluidics 8:054114

Lanotte L, Mauer J, Mendez S, Fedosov DA, Fromental JM, Claveria V, Nicoud F, Gompper G, Abkarian M (2016) Red cells' dynamic morphologies govern blood shear thinning under microcirculatory flow conditions. Proc Natl Acad Sci USA 113:13289–13294

Lew VL, Tiffert T, Ginsburg H (2003) Excess hemoglobin digestion and the osmotic stability of Plasmodium falciparum-infected red blood cells. Blood 101:4189–4194

Li J, Dao M, Lim CT, Suresh S (2005) Spectrin-level modeling of the cytoskeleton and optical tweezers stretching of the erythrocyte. Biophys J 88:3707–3719

Li X, Vlahovska PM, Karniadakis GE (2013) Continuum- and particle-based modeling of shapes and dynamics of red blood cells in health and disease. Soft Matter 9:28–37

Lim GHW, Wortis M, Mukhopadhyay R (2002) Stomatocyte-discocyte-echinocyte sequence of the human red blood cell: evidence for the bilayer-couple hypothesis from membrane mechanics. Proc Natl Acad Sci USA 99:16766–16769

Lim YB, Thingna J, Cao J, Lim CT (2017) Single molecule and multiple bond characterization of catch bond associated cytoadhesion in malaria. Sci Rep 7:4208

Marshall BT, Long M, Piper JW, Yago T, McEver RP, Zhu C (2003) Direct observation of catch bonds involving cell-adhesion molecules. Nature 423:190–193

Mauritz JMA, Esposito A, Ginsburg H, Kaminski CF, Tiffert T, Lew VL (2009) The homeostasis of Plasmodium falciparum-infected red blood cells. PLoS Comput Biol 5:e1000339

Miller LH, Baruch DI, Marsh K, Doumbo OK (2002) The pathogenic basis of malaria. Nature 415:673–679

Monaghan JJ (2005) Smoothed particle hydrodynamics. Rep Prog Phys 68:1703–1759

Nagao E, Kaneko O, Dvorak JA (2000) Plasmodium falciparum-infected erythrocytes: qualitative and quantitative analyses of parasite-induced knobs by atomic force microscopy. J Struct Biol 130:34–44

Nash GB, Cooke BM, Marsh K, Berendt A, Newbold C, Stuart J (1992) Rheological analysis of the adhesive interactions of red blood cells parasitized by Plasmodium falciparum. Blood 79:798–807

Noguchi H, Gompper G (2005) Shape transitions of fluid vesicles and red blood cells in capillary flows. Proc Natl Acad Sci USA 102:14159–14164

Park YK, Diez-Silva M, Popescu G, Lykotrafitis G, Choi W, Feld MS, Suresh S (2008) Refractive index maps and membrane dynamics of human red blood cells parasitized by Plasmodium falciparum. Proc Natl Acad Sci USA 105:13730–13735

Park YK, Best CA, Auth T, Gov NS, Safran SA, Popescu G, Suresh S, Feld MS (2010) Metabolic remodeling of the human red blood cell membrane. Proc Natl Acad Sci USA 107:1289–1294

Peng Z, Mashayekh A, Zhu Q (2014) Erythrocyte responses in low-shear-rate flows: effects of non-biconcave stress-free state in the cytoskeleton. J Fluid Mech 742:96–118

Pivkin IV, Caswell B, Karniadakis GE (2011) Dissipative particle dynamics. In: Lipkowitz KB (ed) Reviews in computational chemistry, vol 27. Wiley, Hoboken, pp 85–110

Pivkin IV, Peng Z, Karniadakis GE, Buffet PA, Dao M, Suresh S (2016) Biomechanics of red blood cells in human spleen and consequences for physiology and disease. Proc Natl Acad Sci USA 113:7804–7809

Popescu G, Park YK, Dasari RR, Badizadegan K, Feld MS (2007) Coherence properties of red blood cell membrane motions. Phys Rev E 76:031902

Pries AR, Neuhaus D, Gaehtgens P (1992) Blood viscosity in tube flow: dependence on diameter and hematocrit. Am J Physiol 263:H1770–H1778

Puig-de-Morales-Marinkovic M, Turner KT, Butler JP, Fredberg JJ, Suresh S (2007) Viscoelasticity of the human red blood cell. Am J Physiol 293:C597–C605

Quadt KA, Barfod L, Andersen D, Bruun J, Gyan B, Hassenkam T, Ofori MF, Hviid L (2012) The density of knobs on Plasmodium falciparum-infected erythrocytes depends on developmental age and varies among isolates. PLoS ONE 7:e45658

Raventos-Suarez C, Kaul DK, Macaluso F, Nagel RL (1985) Membrane knobs are required for the microcirculatory obstruction induced by Plasmodium falciparum-infected erythrocytes. Proc Natl Acad Sci USA 82:3829–3833

Rieger H, Yoshikawa HY, Quadt K, Nielsen MA, Sanchez CP, Salanti A, Tanaka M, Lanzer M (2015) Cytoadhesion of Plasmodium falciparum-infected erythrocytes to chondroitin-4-sulfate is cooperative and shear enhanced. Blood 125:383–391

Seifert U, Berndl K, Lipowsky R (1991) Shape transformations of vesicles: phase diagram for spontaneous curvature and bilayer-coupling models. Phys Rev A 44:1182–1202

Seung HS, Nelson DR (1988) Defects in flexible membranes with crystalline order. Phys Rev A 38:1005–1018

Shelby JP, White J, Ganesan K, Rathod PK, Chiu DT (2003) A microfluidic model for single-cell capillary obstruction by Plasmodium falciparum-infected erythrocytes. Proc Natl Acad Sci USA 100:14618–14622

Shi H, Liu Z, Li A, Yin J, Chong AGL, Tan KSW, Zhang Y, Lim CT (2013) Life cycle-dependent cytoskeletal modifications in Plasmodium falciparum infected erythrocytes. PLoS ONE 8:e61170

Strey H, Peterson M, Sackmann E (1995) Measurement of erythrocyte membrane elasticity by flicker eigenmode decomposition. Biophys J 69:478–488

Suresh S, Spatz J, Mills JP, Micoulet A, Dao M, Lim CT, Beil M, Seufferlein T (2005) Connections between single-cell biomechanics and human disease states: gastrointestinal cancer and malaria. Acta Biomater 1:15–30

Turlier H, Fedosov DA, Audoly BA, Auth T, Gov NS, Sykes C, Joanny JF, Gompper G, Betz T (2016) Equilibrium physics breakdown reveals the active nature of red blood cell membrane fluctuations. Nat Phys 12:513–519

Waldecker M, Dasanna AK, Lansche C, Linke M, Srismith S, Cyrklaff M, Sanchez CP, Schwarz US, Lanzer M (2017) Differential time-dependent volumetric and surface area changes and delayed induction of new permeation pathways in p. falciparum-infected hemoglobinopathic erythrocytes. Cell Microbiol 19:e12650

Waugh R, Evans EA (1979) Thermoelasticity of red blood cell membrane. Biophys J 26:115–131

Wells R, Schmid-Schönbein H (1969) Red cell deformation and fluidity of concentrated cell suspensions. J Appl Physiol 27:213–217

Wendt JF (ed) (2009) Computational fluid dynamics, 3rd edn. Springer, Berlin

Wu T, Feng JJ (2013) Simulation of malaria-infected red blood cells in microfluidic channels: passage and blockage. Biomicrofluidics 7:044115

Yipp BG, Anand S, Schollaardt T, Patel KD, Looareesuwan S, Ho M (2000) Synergism of multiple adhesion molecules in mediating cytoadherence of Plasmodium falciparum-infected erythrocytes to microvascular endothelial cells under flow. Blood 96:2292–2298

Zhang Y, Huang C, Kim S, Golkaram M, Dixon MWA, Tilley L, Li J, Zhang S, Suresh S (2015) Multiple stiffening effects of nanoscale knobs on human red blood cells infected with Plasmodium falciparum malaria parasite. Proc Natl Acad Sci USA 112:6068–6073